

## Huygens-Fresnel Picture for High Harmonic Generation in Solids

Liang Li,<sup>1</sup> Pengfei Lan,<sup>1,\*</sup> Xiaosong Zhu,<sup>1</sup> and Peixiang Lu<sup>1,2,3,†</sup>

<sup>1</sup>Wuhan National Laboratory for Optoelectronics and School of Physics, Huazhong University of Science and Technology, Wuhan 430074, China

<sup>2</sup>Hubei Key Laboratory of Optical Information and Pattern Recognition, Wuhan Institute of Technology, Wuhan 430205, China

<sup>3</sup>CAS Center for Excellence in Ultra-intense Laser Science, Shanghai 201800, China



(Received 23 April 2021; accepted 26 October 2021; published 22 November 2021)

High harmonic generation (HHG) is usually described by the laser-induced recollision of particlelike electrons, which lies at the heart of attosecond physics and also inspires numerous attosecond spectroscopic methods. Here, we demonstrate that the wavelike behavior of electrons plays an important role in solid HHG. By taking an analogy to the Huygens-Fresnel principle, an electron wave perspective on solid HHG is proposed by using the wavelet stationary-phase method. From this perspective, we have explained the deviation between the cutoff law predicted by the particlelike recollision model and the numerical simulation of semiconductor Bloch equations. Moreover, the emission times of HHG can be well predicted with our method involving the wave property of electrons. However, in contrast, the prediction with the particlelike recollision model shows obvious deviations compared to the semiconductor Bloch equations simulation. The wavelike properties of the electron motion can also be revealed by the HHG in a two-color field.

DOI: [10.1103/PhysRevLett.127.223201](https://doi.org/10.1103/PhysRevLett.127.223201)

Laser-induced recollision [1–5] provides an intuitive picture for many strong-field phenomena, e.g., high harmonic generation (HHG) [6–8], high-order above-threshold ionization [9,10], and nonsequential double ionization [11,12], and plays a vital role in attosecond physics. Following the recollision picture, classical and semiclassical trajectory-based models have been developed [13–17]. The recollision picture has made a big success to understand the strong-field physics in the past three decades [18,19]. On the other hand, it also inspires the novel approaches toward elucidating the time-resolved dynamics of atoms and molecules through the techniques of laser-induced electron diffraction (LIED) [20–24] and high harmonic spectroscopy (HHS) [25–30].

The recent process of attosecond science has been extended to solid systems [31–38]. Following the big success in gases, solid HHG is usually also explained with the recollision picture [39,40], i.e., the electron in the valence band (VB) is first excited to the conduction band (CB) and then accelerated by the laser field and finally recombined with the hole. In this context, the electron behavior is generally modeled by the particlelike motion. Similar to the HHG in gases, one can expect the extension of attosecond techniques to solids if an internal clock capable of resolving ultrafast dynamics on an attosecond timescale is provided [33–35]. From the particlelike recollision picture, this internal clock is always established by the electron-hole recombination events. As is well known, wave-particle duality is the elementary nature of the quantum process. The electron is much less localized in

solids compared to that in gases. Moreover, the solid systems always have complicated band structures and thus have different dispersions when an electron moves following the energy bands. Indeed, some works have modified the saddle-point equations or recollision conditions by taking account of the width or separation of electron and hole wave packets [41–43]. However, the harmonic emission is still described by the trajectory-based recollisions formulated by the saddle-point equations, and the coherence and interference of the electron wave packet during propagation is excluded. It is important to ask whether the particlelike recollision picture still works well in solids. If not, how does one establish the internal clock in the relevant spectroscopic methods, e.g., HHS or LIED? To address these questions, a comprehensive picture involving the wave properties of electrons in solid HHG is indispensable.

In this Letter, we focus on the wavelike behavior of electrons in solid HHG. Different from the particlelike recollision picture, we propose a wave perspective on solid HHG. It is shown that the spectrotemporal characteristics of solid HHG cannot be accurately described by the recollision picture and that the wave properties of the electron motion play an important role. The emission time predicted with the recollision model could deviate about 500 attoseconds from the simulations with semiconductor Bloch equations (SBEs). In contrast, we propose a different procedure to establish the time-energy correspondences of solid HHG according to our model, and the spectrotemporal characteristics, e.g., the emission time and cutoff law,

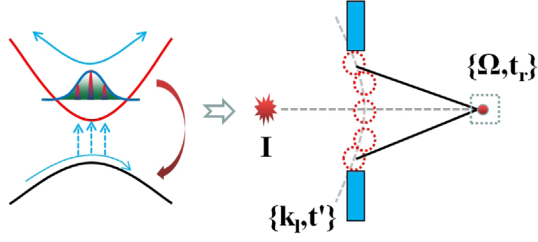


FIG. 1. Sketch for HHG analogy to the Huygens-Fresnel principle.

can be well reproduced. Our work provides a comprehensive picture for solid HHG and also paves the way to attosecond spectroscopy in solids.

Our wavelike perspective of solid HHG is obtained by an analogy to the Huygens-Fresnel principle (see Fig. 1). At the ionization time  $t'$ , the electron wave packet ionized by the laser field is treated as a composition of wavelets, just like the secondary wavelets in the Huygens-Fresnel principle. Each wavelet is denoted as  $\{k_l, t_l\}$ , where  $k_l$  is the central momentum of the electron wavelet. The harmonic emission at time  $t_r$ , just like the wave at the observation in the Huygens-Fresnel principle, can be described by the interference of the contributions from all wavelets. If the diffraction during the propagation can be neglected, one can treat the electron as a particle, which is similar to geometrical-optics approximation. In this case, the electron motion can be described by classical trajectories following the saddle-point equations. However, due to the delocalization of the electron wave packet and complicated dispersion of the band structure in solids, the electron wave packet will be dramatically distorted during the evolution (see section B in the Supplemental Material (SM) [44]). Therefore, the wave properties of electrons have to be considered and the electron motion should be described by a series of wavelets rather than particles.

Our analysis of the laser-solids interaction is based on a two-band model [39–43]. We consider a filled VB and an empty CB over the first Brillouin zone (BZ). Within the

parameters used in this work, the contribution of the intraband current is much lower than the interband current for the HHG above the band gap; therefore, we only consider the interband current in the following discussion. The interband current can be derived as in Ref. [45], which is demonstrated to agree well with that in Refs. [39,40] (see also section A in the SM [44]),

$$J_{\text{er}}(t) = - \int_{\text{BZ}} dk' \int_{-\infty}^t dt' I(k', t') e^{-iS(k', t, t')} R(k', t, t') + \text{c.c.} \quad (1)$$

In Eq. (1), we use the notations  $I(k', t') = F(t') \cdot X_{cv}(k')$ ,  $S(k', t, t') = \int_{t'}^t \Delta \varepsilon_{cv}[k(k', \tau, t')] d\tau$ , and  $R(k', t, t') = \Delta \varepsilon_{cv}[k(k', t, t')] X_{cv}[k(k', t, t')]$ , where  $X_{cv}(k) = \langle u_{ck} | i \nabla_k | u_{vk} \rangle$  is the transition dipole moment.  $|u_{vk}\rangle$  and  $|u_{ck}\rangle$  are the periodic part of the Bloch functions,  $\Delta \varepsilon_{cv} = \varepsilon_c - \varepsilon_v$  is the gap energy between the CB and VB, and  $k(k', t, t') = k' + A(t) - A(t')$  is a reciprocal-space trajectory ionized from  $k'$  [45]. Here, we present the formula in the one dimensional case, and it can be easily extended to three dimensions. It is worthy to note that the saddle-point approximation does not always work well for the integrals in Eq. (1) due to the electron delocalization and complicated dispersion (see section B in the SM [44]). To overcome this problem, we propose a Gaussian wavelet method following Huygens-Fresnel principle.

As sketched in Fig. 1, we separate the electron wave packet into a series of Gaussian wavelets  $g(k', k_l, t') = e^{-\{k' - k_l \cdot \text{sign}[F(t')]\}^2 / k_w^2}$ . In this form,  $k_l > 0$  indicates the wavelets ionized along the same direction as the electric field, while  $k_l < 0$  indicates the wavelet ionized antiparallel to the electric field. The corresponding weight coefficient  $f(k_l, t')$  satisfies  $I(k', t') = \sum_{k_l} f(k_l, t') g(k', k_l, t')$ .  $k_w$  is the width of the Gaussian wavelets. Then, the harmonic emission at time  $t_r$  can be expressed by a coherent superposition of the contributions from different wavelets,

$$\begin{aligned} Y(\Omega, t_r) &\propto \left| \int_{-\infty}^{+\infty} J_{\text{er}}(t) [w(t, t_r) e^{i\Omega t}]^2 \right| \\ &= \left| \sum_{k_l, t'} f(k_l, t') \int_{-\infty}^{+\infty} \int_{-\infty}^{+\infty} dt dk' g(k', k_l, t') e^{-iS(k', t, t')} R(k', t, t') [w(t, t_r) e^{i\Omega t}]^2 \right|, \end{aligned} \quad (2)$$

where  $(\Omega, t_r)$  is the angular frequency and emission time of HHG (i.e., the observation point in the Huygens-Fresnel principle), and  $w(t, t_r) = e^{-(t-t_r)^2/t_w^2}$  is a time window near the observation point.

We adopt the Gaussian integral, and the integration over  $t$  and  $k'$  in Eq. (2) can be expressed as (see section C in the SM [44])

$$D(k_l, t_r, t') = e^{-iS(k_l, t_r, t') + i\Omega t_r} G[\partial_{k'} S(k_l, t_r, t'), \Delta x] W[\partial_t S(k_l, t_r, t') - \Omega, \Delta E] R(k_l, t_r, t'), \quad (3)$$

where  $G[\partial_{k'}S(k_l, t_r, t'), \Delta x] = k_w \sqrt{\pi} \exp\{-[(\partial_{k'}S(k_l, t_r, t'))/(\Delta x)]^2\}$  and  $W[\partial_{t'}S(k', t_r, t') - \Omega, \Delta E] = t_w \sqrt{\pi} \times \exp\{-[(\partial_{t'}S(k', t_r, t') - \Omega)/(\Delta E)]^2\}$ . Note that  $D(k_l, t_r, t')$  describes the emission pulse around  $\{\Omega, t_r\}$ .  $\Delta E = 2/t_w$  and  $\Delta x = 2/k_w$  denote the width of the emission.

By substituting Eq. (3) into Eq. (2), the harmonic yield can be rewritten as

$$Y(\Omega, t_r) \propto \left| \sum_{k_l, t' \in [0, t_r]} f(k_l, t') D(k', t_r, t') \right|^2 = \left| \sum_{k_l, t' \in [0, t_r]} f(k_l, t') P(k_l, t_r, t') e^{-iS(k_l, t_r, t')} \right|^2, \quad (4)$$

where  $P(k_l, t_r, t') = G[\partial_{k'}S(k_l, t_r, t'), \Delta x] W[\partial_{t'}S(k_l, t_r, t') - \Omega, \Delta E] R(k_l, t_r, t')$  describes the emission pulse of a single wavelet and  $e^{-iS(k_l, t_r, t')}$  is the corresponding phase. For the summation over  $t'$ , the constructive interference at the observation point  $(\Omega, t_r)$  occurs when the phase changes most slowly, i.e.,  $|\partial_{t'}S| = |\Delta \varepsilon_{cv}(k_l) - x(k_l, t_r, t') F(t')|$  reaches minimum.  $x(k', t, t') = \int_{t'}^t \{\partial_k \Delta \varepsilon_{cv}[k' + A(\tau) - A(t')]\} d\tau$  indicates the effective electron-hole displacement.

Note that the HHG in previous works is described by the particlelike recollision picture based on saddle-point equations [39–43]. We call it the classical saddle-point method (CSPM) in the following discussions. Different from that, the HHG in our model is described by the interference of a series of wavelet contributions [Gaussian distribution P in Eq. (4)] and the most probable ionization time  $t_i$  is determined by the constructive interference at  $\{t_i | \min[|\partial_{t'}S(k_l, t_r, t')|]\}$ . We call it the wavelet stationary-phase method (WSPM). As will be shown below,  $|\partial_{t'}S|$  does not always reach zero in solid HHG; therefore, we choose the condition reaching its minimum. Moreover, for each wavelet, the emissions are described by Gaussian distributions with the uncertainties  $\Delta x$  and  $\Delta E$  rather than a single harmonic at a certain time (i.e., delta functions). These uncertainties come from the Fourier limit by considering the wave properties of electrons.

In our model, the correspondence between the microdynamics and harmonic emissions is established by considering the most probable distribution at the observation point  $\{\Omega, t_r\}$  (see Fig. 2). This relation is different from that obtained by saddle-point equations [39–43] because we use exact Gaussian integrations rather than a saddle-point approximation when dealing with the contributions of different paths. In our model, the wave properties are inherently embedded in the evolution of the Gaussian wavelets. Note that particlelike recollision picture obtained from the CSPM can be reproduced in the quasiparticle limit, i.e.,  $\Delta x \rightarrow 0$  and  $\Delta E \rightarrow 0$ . This indicates the intrinsic consistency between our model and the previous CSPM.

To demonstrate the wavelike property, we discuss the HHG of ZnO crystals in a near-infrared laser field. We use the same parameters as Refs. [39,40] and concentrate on the

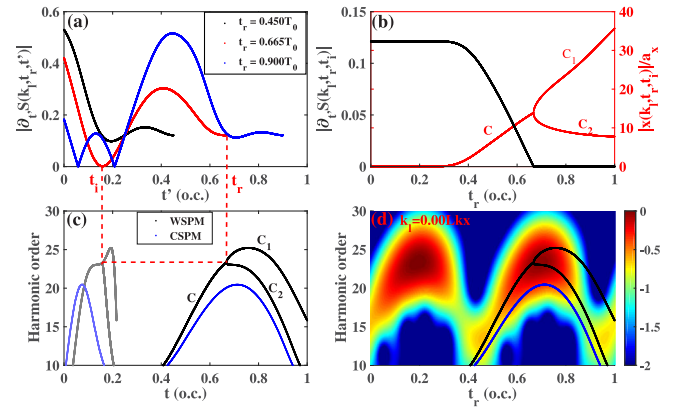


FIG. 2. Time frequency property of HHG for the channel  $k_l = 0$ . (a) The absolute value of partial derivative of quasiclassical action  $|\partial_{t'}S(k_l, t_r, t')|$  for the different emission times  $t_r = 0.0450 T_0$ ,  $0.665 T_0$ , and  $0.900 T_0$ . (b) The values  $|\partial_{t'}S(k_l, t_r, t_i)|$  (black line) and effective electron-hole displacement  $|x(k_l, t_r, t_i)/a_x|$  (red line) with  $t_i$  determined by Fig. 2(a). (c) The relation between the most probable emission energy and emission (ionization) times. The gray and black lines are obtained with our WSPM method. The light blue and blue lines are obtained with the CSPM method. (d) The time frequency property of HHG obtained with the numerical integration of Eq. (2). The black line and blue line are the results obtained with the WSPM and CSPM.

linearly polarized laser field along the axis  $\Gamma$ – $M$ . The laser pulse has a sine squared envelope with a duration of ten optical cycles  $10 T_0$ , and the amplitude  $F_0 = 0.003$  a.u. The laser frequency  $\omega_0 = 0.0152$  a.u., which corresponds to the wavelength of 3000 nm.  $t = 0$  corresponds to the pulse center. The dephasing effect is phenomenally involved by introducing an attenuation term  $e^{-(t_r - t')/T_2}$  into the interband current with  $T_2 = 0.25 T_0$ . The SBES and CSPM analyses are performed following the methods in Refs. [39,40]. The comparison between the SBES simulations and the integrations in Eq. (1) shows that the HHG is mainly contributed by the channels ionized near the  $\Gamma$  point of ZnO (see section D in the SM [44]). Thus, one can reduce the simulations for channels  $|k_l| < 0.05 L_{kx}$ , where  $L_{kx}$  is the width of the first BZ. The width of each wavelet is  $0.01 L_{kx}$ .

First, we analyze the quantum path for one single channel  $k_l = 0$ . In Fig. 2(a), we plot the absolute value of partial derivative of quasiclassical action with respect to  $t'$ , i.e.,  $|\partial_{t'}S|$ . The location of each line's tail corresponds to the emission time  $t_r$ . According to Eq. (4), the position of the minimum corresponds to the most probable ionization time  $t_i$ . Then, one can determine the central frequency of the emission by  $\Omega = \Delta \varepsilon_{cv}(k_l, t_r, t_i)$ , which is the peak location of the harmonic yield  $Y_{k_l}(\Omega, t_r)$ . For example, the red line in Fig. 2(a) indicates the emission time  $t_r = 0.665 T_0$  and the ionization time  $t_i = 0.17 T_0$ . Following this procedure, one can obtain the relation between the emission energy and emission (ionization) time. The results

are shown in Fig. 2(c). For comparison, the blue lines obtained with the CSPM are also plotted. Different from the CSPM, the WSPM indicates three types of paths: “C”, “C<sub>1</sub>”, and “C<sub>2</sub>”. For  $t_r < 0.665 T_0$ , one can see that  $|\partial_r S|$  is always larger than 0. There is only one minimum, and its trace forms the path “C”, which is similar to the short trajectory in CSPM. In contrast, for  $t_r > 0.665 T_0$ , there are two minima, which correspond to the paths “C<sub>1</sub>”, and “C<sub>2</sub>”. We show the value of  $|\partial_r S(k_l, t_r, t_i)|$  and the effective electron-hole displacement  $|x(k_l, t_r, t_i)|/a_x$  in Fig. 2(b). Note that we only discuss the results for  $t_r > 0.4 T_0$ , because the contribution with smaller  $t_r$  is negligible for the interband HHG. As shown in Fig. 2(b), the effective electron-hole displacement  $|x(k_l, t_r, t_i)|$  is always deviated from 0. In other words, the recollision condition in the CSPM,  $|x(k_l, t_r, t_i)| = 0$ , is broken. This can be understood by the delocalized electron wave packet propagating with nonparabolic energy dispersion. In this case, the most probable emission time as well as the effective electron-hole displacement are modified by the distortion of the electron wave packet. Besides, the relative displacement of path “C<sub>1</sub>” is obviously larger than those of paths “C” and “C<sub>2</sub>”; its contribution is much less than the paths “C” and “C<sub>2</sub>” by considering the spread of Gaussian wavelets.

For comparison, Fig. 2(d) shows the numerical results of Eq. (2) for the channel  $k_l = 0$ . One can see that the path obtained from the WSPM well describes the time-frequency features of the HHG. Following the discussions above, one can obtain the relation between the emission energy and emission time for different channels, e.g.,  $k_l = 0.02 L_{\text{KX}}$ , and  $k_l = 0.04 L_{\text{KX}}$  in Figs. 3(a) and 3(b). Here, we only show the dominant channels with  $k_l > 0$  (see

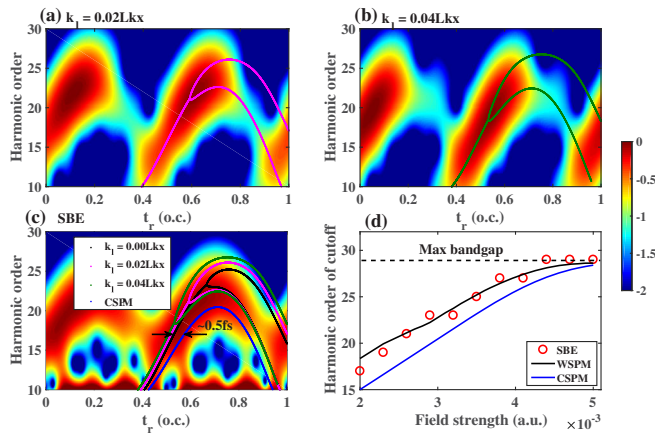


FIG. 3. The time frequency property of HHG from the numerical results for channels (a)  $k_l = 0.02 L_{\text{KX}}$ , and (b)  $k_l = 0.04 L_{\text{KX}}$ . (c) The result for SBEs. The WSPM results are marked by black, purple, and green dots that are copies from Figs. 2(d), 3(a), and 3(b). The CSPM result is marked by blue points. (d) The simulated cutoff law (red circles); the prediction from WSPM (solid black line) and CSPM (blue line).

section E in the SM [44] for channels with  $k_l < 0$ ). One can see the bifurcation structure near the cutoff, which supports the prediction of two paths C<sub>1</sub> and C<sub>2</sub> with the WSPM. For comparison, the time-frequency property obtained with SBEs is shown in Fig. 3(c). One can see that all the paths predicted with the WSPM have a similar trend and are in good agreement with the SBEs simulation. However, the CSPM predictions have nearly 0.5 fs deviations from the SBEs simulation. More importantly, the WSPM predicts a higher cutoff energy than that from the CSPM. Note that we neglect the path C<sub>1</sub> because of its weak contribution (see Fig. 3 in the SM [44]), and the cutoff energy is determined by the paths C and C<sub>2</sub>. As shown in Fig. 3(d), the higher cutoff agrees well with the SBEs simulation [see Fig. 3(d)]. This result explains the long-standing deviation about the cutoff law between the CSPM and the SBEs simulation [40] and also demonstrates the influence of the wavelike properties predicted by our model.

The recollision picture has also inspired the development of attosecond spectroscopy in gases, where the key is the timeline defined by the relation between the harmonic energy and emission (or ionization) time. However, the wavelike behavior of the electron motion in solids will dramatically influence such a relation. To show this effect, we consider a simulation experiment of HHG interferometry formed by a fundamental pulse ( $A_{\omega_0}$ ) with a perturbative second harmonic field ( $A_{2\omega_0}$ ) [33,46]. The second harmonic perturbs the quantum path differently in the adjacent half cycle. It forms interferometry with two unbalanced arms and will lead to the generation of even harmonics. When the second harmonic is much weaker than the fundamental field, the even harmonic yields  $Y(t, \phi, k_l) \propto \sin^2[\sigma(t, \phi)] \sim \sigma^2(t, \phi)$ , where

$$\begin{aligned} \sigma(t, \phi) &= \int_{t'(t)}^t v[k_l - A_{\omega_0}(t') + A_{\omega_0}(\tau)] \\ &\quad \times [A_{2\omega_0}(\tau, \phi) - A_{2\omega_0}(t', \phi)] d\tau \\ &= \sigma_s(t) \cos(\phi) + \sigma_c(t) \sin(\phi) = \Sigma(t) \cos[\phi - \theta(t)]. \end{aligned} \quad (5)$$

In this equation,  $\sigma_s(t) = A_2 \int_{t'(t)}^t v[k_l - A_{\omega_0}(t') + A_{\omega_0}(\tau)] \times [\sin(2\omega_0\tau) - \sin(2\omega_0t')] d\tau$ ,  $\sigma_c(t) = A_2 \int_{t'(t)}^t v[k_l - A_{\omega_0}(t') + A_{\omega_0}(\tau)] [\cos(2\omega_0\tau) - \cos(2\omega_0t')] d\tau$ ,  $\theta(t) = \arctan(\sigma_c/\sigma_s)$ , and  $\Sigma(t) = \sqrt{\sigma_c^2 + \sigma_s^2}$ . Thus, the even harmonic reaches the maximum at the relative phase  $\phi_{\text{max}}(t_{2N}) \equiv \theta(t_{2N})$ , where  $t_{2N}$  is the emission time of the  $2N$ th harmonic. Note that, different from the CSPM, the terms contributed by  $A_{2\omega_0}(t', \phi)$  in the integration should be maintained because the effective electron-hole displacement  $|x(k_l, t_r, t')|$  are always nonzero as shown in Fig. 2(b).

Figure 4(b) shows the phase dependence of HHG spectra simulated with SBEs. For clarity, the yield of each order harmonic is normalized to 1. The blue line is obtained by

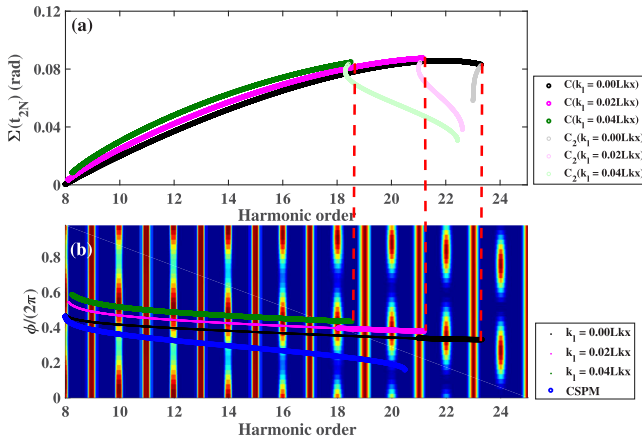


FIG. 4. (a) The value of  $\Sigma(t_{2N})$  for different channels. (b) Simulated spectrum for HHG. Each harmonic order has been normalized to simplify comparison. The laser parameters are  $\omega = 0.0152$  a.u.,  $F_0 = 0.003$  a.u., and  $F_{2\omega_0} = 0.01 F_0$ .

using the CSPM. There is a deviation of nearly  $0.4\pi$  ( $\sim 1$  fs) between the CSPM prediction and the SBEs simulation. Such a deviation can lead to a large error or even prevent one from correctly retrieving the subcycle dynamics with HHS. The deviation between the CSPM and SBEs is mainly due to the deformation of the electron wave packet. In other words, after ionization, the Gaussian electron wave packet moves in the CB driven by the laser field. However, the energy dispersion of the solid is no longer a parabola with a constant effective mass. The electron wave packet will be distorted due to the mismatch between the phase velocity and group velocity (see Fig. 2 in the SM [44]). Such an effect will blur the recollision event and cannot be correctly modeled in the particlelike recollision picture. In contrast, our model includes the wave properties of the electron. As shown in Fig. 4(b), the  $\phi_{\max}$  predicted by our WSPM agrees very well with the SBEs. Moreover, there is more than one channel and different harmonics are contributed by different channels. In Fig. 4(a), we plot the fringe amplitudes  $\Sigma(t_{2N})$  for different channels. One can see that the cutoff of path “C” is increased with reducing the  $k_l$  and the contribution of “C<sub>2</sub>” is less obvious. The dominant channel is shifted from  $k_l = 0.04 L_{kx}$  to  $k_l = 0.02 L_{kx}$  and  $k_l = 0$  with increasing the harmonic order. For the high harmonics from 8th to 18th, the dominant channel is  $k_l = 0.04 L_{kx}$ , and  $\phi_{\max}$  decreases slowly with increasing the harmonic order. Then,  $\phi_{\max}$  decreases slightly faster from the 20th to 24th harmonics, which can be attributed to the dominant contribution of channels  $k_l = 0.02 L_{kx}$  and  $k_l = 0$ .

In conclusion, we proposed an electron wave perspective on solid HHG by taking account of the similarity between the propagation of the electron wave packet and the optical pulse. Compared to the particlelike recollision picture, our model provides a different and complementary perspective for understanding the HHG. The wavelike behavior plays a

significant role in solid HHG due to the nonparabolic band structure and delocalized electron wave packet. The emission time and cutoff energy of the HHG are shifted by considering the wave properties of the electron motion. The prediction by our model agrees well with the SBEs simulations. However, in contrast, the emission time predicted by the CSPM deviates 500 attoseconds from the SBEs simulation. This effect will have a substantial impact on the attosecond metrology and the wavelike properties have to be considered when extending the attosecond spectroscopy, e.g., HHS, LIED, from gases to solids.

This Letter was supported by the National Key R&D program (2017YFE0116600) and National Natural Science Foundation of China (NSFC) (No. 11934006, No. 91950202, No. 11627809, No. 12021004, No. 11874165). We acknowledge C. D. Lin and M. Lein for reading the manuscript.

\*Corresponding author.  
pengfeilan@hust.edu.cn

†Corresponding author.  
lupeixiang@hust.edu.cn

- [1] P. B. Corkum, *Phys. Rev. Lett.* **71**, 1994 (1993).
- [2] J. L. Krause, K. J. Schafer, and K. C. Kulander, *Phys. Rev. Lett.* **68**, 3535 (1992).
- [3] M. Lewenstein, P. Balcou, M. Y. Ivanov, A. L’Huillier, and P. B. Corkum, *Phys. Rev. A* **49**, 2117 (1994).
- [4] P. Salières, B. Carré, L. Le Déroff, F. Grasbon, G. G. Paulus, H. Walther, R. Kopold, W. Becker, D. B. Milošević, A. Sanpera, and M. Lewenstein, *Science* **292**, 902 (2001).
- [5] A.-T. Le, R. R. Lucchese, S. Tonzani, T. Morishita, and C. D. Lin, *Phys. Rev. A* **80**, 013401 (2009).
- [6] J. Itatani, J. Levesque, D. Zeidler, H. Niikura, H. Pépin, J. C. Kieffer, P. B. Corkum, and D. M. Villeneuve, *Nature (London)* **432**, 867 (2004).
- [7] C. I. Blaga, J. Xu, A. D. DiChiara, E. Sistrunk, K. Zhang, P. Agostini, T. A. Miller, L. F. DiMauro, and C. D. Lin, *Nature (London)* **483**, 194 (2012).
- [8] M. G. Pullen *et al.*, *Nat. Commun.* **6**, 7262 (2015).
- [9] D. B. Milošević, G. G. Paulus, D. Bauer, and W. Becker, *J. Phys. B* **39**, R203 (2006).
- [10] W. Becker, S. P. Goreslavski, D. B. Milošević, and G. G. Paulus, *J. Phys. B* **51**, 162002 (2018).
- [11] C. F. de Morisson Faria and X. Liu, *J. Mod. Opt.* **58**, 1076 (2011).
- [12] W. Becker, X. J. Liu, P. J. Ho, and J. H. Eberly, *Rev. Mod. Phys.* **84**, 1011 (2012).
- [13] J. Chen, J. Liu, L. B. Fu, and W. M. Zheng, *Phys. Rev. A* **63**, 011404(R) (2000).
- [14] J. Wu, B. Augstein, and C. Figueira de Morisson Faria, *Phys. Rev. A* **88**, 063416 (2013).
- [15] A. Kamor, C. Chandre, T. Uzer, and F. Mauger, *Phys. Rev. Lett.* **112**, 133003 (2014).
- [16] K. Schafer, Z. Wei, and M. Vrakking, *J. Phys. B* **50**, 170201 (2017).
- [17] D. B. Milošević, *Phys. Rev. A* **96**, 023413 (2017).

- [18] K. Schafer, Z. Wei, and M. Vrakking, *J. Phys. B* **50**, 170201 (2017).
- [19] K. Amini *et al.*, *Rep. Prog. Phys.* **82**, 116001 (2019).
- [20] T. Zuo, A. D. Bandrauk, and P. B. Corkum, *Chem. Phys. Lett.* **259**, 313 (1996).
- [21] S. N. Yurchenko, S. Patchkovskii, I. V. Litvinyuk, P. B. Corkum, and G. L. Yudin, *Phys. Rev. Lett.* **93**, 223003 (2004).
- [22] T. Morishita, A. T. Le, Z. Chen, and C. D. Lin, *Phys. Rev. Lett.* **100**, 013903 (2008).
- [23] J. Xu, C. I. Blaga, A. D. DiChiara, E. Sistrunk, K. Zhang, Z. Chen, A.-T. Le, T. Morishita, C. D. Lin, P. Agostini, and L. F. DiMauro, *Phys. Rev. Lett.* **109**, 233002 (2012).
- [24] B. Wolter *et al.*, *Science* **354**, 308 (2016).
- [25] S. Baker, J. S. Robinson, C. A. Haworth, H. Teng, R. A. Smith, C. C. Chirilă, M. Lein, J. W. G. Tisch, and J. P. Marangos, *Science* **312**, 424 (2006).
- [26] O. Smirnova, Y. Mairesse, S. Patchkovskii, N. Dudovich, D. Villeneuve, P. Corkum, and M. Y. Ivanov, *Nature (London)* **460**, 972 (2009).
- [27] S. Haessler, J. Caillat, W. Boutou, C. Giovanetti-Teixeira, T. Ruchon, T. Auguste, Z. Diveki, P. Breger, A. Maquet, B. Carre, R. Taieb, and P. Salieres, *Nat. Phys.* **6**, 200 (2010).
- [28] C. Vozzi, M. Negro, F. Calegari, G. Sansone, M. Nisoli, S. De Silvestri, and S. Stagira, *Nat. Phys.* **7**, 822 (2011).
- [29] P. M. Kraus *et al.*, *Science* **350**, 790 (2015).
- [30] P. Lan, M. Ruhmann, L. He, C. Zhai, F. Wang, X. Zhu, Q. Zhang, Y. Zhou, M. Li, M. Lein, and P. Lu, *Phys. Rev. Lett.* **119**, 033201 (2017).
- [31] S. Ghimire, A. D. DiChiara, E. Sistrunk, P. Agostini, L. F. DiMauro, and D. A. Reis, *Nat. Phys.* **7**, 138 (2011).
- [32] T. T. Luu, M. Garg, S. Y. Kruchinin, A. Moulet, M. T. Hassan, and E. Goulielmakis, *Nature (London)* **521**, 498 (2015).
- [33] G. Vampa, T. J. Hammond, N. Thiré, B. E. Schmidt, F. Légaré, C. R. McDonald, T. Brabec, and P. B. Corkum, *Nature (London)* **522**, 462 (2015).
- [34] F. Langer *et al.*, *Nature (London)* **533**, 225 (2016).
- [35] H. B. Banks, Q. Wu, D. C. Valocin, S. Mack, A. C. Gossard, L. Pfeiffer, R. B. Liu, and M. S. Sherwin, *Phys. Rev. X* **7**, 041042 (2017).
- [36] A. von Hoegen, R. Mankowsky, M. Fechner, M. Först, and A. Cavalleri, *Nature (London)* **555**, 79 (2018).
- [37] S. Jiang, J. Chen, H. Wei, C. Yu, R. Lu, and C. D. Lin, *Phys. Rev. Lett.* **120**, 253201 (2018).
- [38] A. J. Uzan *et al.*, *Nat. Photonics* **14**, 183 (2020).
- [39] G. Vampa, C. R. McDonald, G. Orlando, D. D. Klug, P. B. Corkum, and T. Brabec, *Phys. Rev. Lett.* **113**, 073901 (2014).
- [40] G. Vampa, C. R. McDonald, G. Orlando, P. B. Corkum, and T. Brabec, *Phys. Rev. B* **91**, 064302 (2015).
- [41] E. N. Osika, A. Chacón, L. Ortmann, N. Suárez, J. A. Pérez-Hernández, B. Szafran, M. F. Ciappina, F. Sols, A. S. Landsman, and M. Lewenstein, *Phys. Rev. X* **7**, 021017 (2017).
- [42] L. Yue and M. B. Gaarde, *Phys. Rev. Lett.* **124**, 153204 (2020).
- [43] A. M. Parks, G. Ernotte, A. Thorpe, C. R. McDonald, P. B. Corkum, M. Taucer, and T. Brabec, *Optica* **7**, 1764 (2020).
- [44] See Supplemental Material at <http://link.aps.org/supplemental/10.1103/PhysRevLett.127.223201> for detailed derivations and more discussions.
- [45] L. Li, P. Lan, X. Zhu, T. Huang, Q. Zhang, M. Lein, and P. Lu, *Phys. Rev. Lett.* **122**, 193901 (2019).
- [46] G. Vampa, J. Lu, Y. S. You, D. R. Baykusheva, M. Wu, H. Liu, K. J. Schafer, M. B. Gaarde, D. A. Reis, and S. Ghimire, *J. Phys. B* **53**, 144003 (2020).